Supplementary Information

1. Experimental section

1.1 Chemical and materials

Nickel phthalocyanine (NiPc) and graphene were purchased from Alfa Aesar. Multi-walled carbon nanotubes were purchased from Tokyo Chemical Industry. N,N-Dimethylformamide (DMF) (99.5%) was obtained from Kermel. Potassium bicarbonate (99.7%) was obtained from Sigma-Aldrich. Nafion solution (Dupont, 5 wt. %). All chemicals were used without any further purification.

1.2 Preparation of various carbon supports

Different types of carbon supports including graphene, carbon nanotubes, XC72 and acetylene black, were used as received. A series of pretreatment processes were performed on these carbon supports to remove metals and ashes. The carbon support was firstly stirred and ultrasonically dispersed in hydrochloric acid (7 vol.%) for 10 minutes with 50 mL hydrochloric acid per gram of carbon support. Subsequently, the suspension was placed in an oil bath at 120 ℃ for 8 hours, washed with deionized water and filtered until the filtrate reached neutral pH, and finally dried in an oven at 120 ℃ for 12 hours.

1.3 Preparation of carbon supported NiPc

20 mg of nickel phthalocyanine (NiPc) was ultrasonically dispersed in 30 mL of N,N-dimethylformamide for 30 minutes, followed by adding 200 mg of carbon support and ultrasonicated for another 30 minutes and then stirred for 48 hours. To remove unsupported NiPc, The stirred solution was first vacuum-filtered with N,N-dimethylformamide 5 times, and then with ethanol 2 times, and then dried in an oven at 60°C for 5 hours.

1.4 CO_2RR gas diffusion electrode (GDE) preparation

10 mg of the catalyst was added into 1 mL solution containing 480 μL isopropanol, 480 μL deionized water, and 40 μL Nafion solution (5 wt.%), and sonicated for 30 minutes to prepare the catalyst ink. The catalyst ink was brushed onto a piece of pretreated carbon paper at 60 ℃ with a catalyst loading of 1.0 $mg \cdot cm^{-2}$ unless

otherwise specified.

1.5 Characterization

The morphological information of the catalyst was examined by scanning electron microscopy (SEM) (Zeiss ORION NanoFab helium ion microscope) and transmission electron microscopy (TEM) (JEOL JEM-2100F transmission electron microscope). The infrared experiments were performed on a Nicolet iS50 spectrometer in the wavenumber range from 500 to 4000 cm^{-1}. Bruker Optics Senterra's dispersive Raman-modified Raman and confocal microscopy system was used. The scanning range is 100-3500 cm^{-1}, the incident light wavelength is 532 nm, and the exposure time is 60 s. The N_2 adsorption was measured on American Mike ASAP 2020 with analysis bath temperature at 77.3 K. The CO_2 adsorption was measured on Quadrasorb S with analysis bath temperature at 273.15 K. Before measurement, the sample was degassed at 110 ℃ for 12 hours. X-ray photoelectron spectroscopy measurements were performed on a Thermo Scientific ESCALAB 250Xi with Al Kα radiation. The CO_2 temperature programmed desorption (TPD) experiment was conducted on a Micromeritics AutoChem II 2920 chemisorption instrument. The content of metal elements in the sample was measured on a Thermal Scientific-IRIS Intrepid II XPS inductively coupled plasma emission spectrometer (ICP-OES).

1.6 Electrochemical measurements

The CO_2RR was tested in a homemade H-type cell separated by a Nafion-115 membrane. The resistance between the reference electrode and the working electrode was measured using electrochemical impedance spectroscopy (EIS) and compensated manually. The electrolyte was a 0.5 M $KHCO_3$ solution (99.5% analytically pure) (pH = 7.3). The reaction temperature was controlled to 25 ℃ by a circulating water pump. During CO_2RR tests, a 500 rpm constant-speed stirring was maintained. The gas Faradaic efficiency were measured under each fixed potential, during one hour controlled potential electrolysis on a Chenhua electrochemical workstation (CHI660E). Controlled potential electrolysis at different applied potentials was shown in Figure S9. Stability test of Ni-G at -0.63 V vs. RHE in 12 hours was conducted and shown in Figure S11. The linear sweep voltammetry (LSV) curve and cyclic

voltammetry (CV) curve were measured on rotating disk electrode (RDE), the rotating speed was set constant at 1500 rpm, all data were corrected for an ohmic drop.

1.6 Quantification of CO_2RR products

The gaseous CO_2RR products were quantified by a gas chromatography (GC7890B), equipped with a flame ionization detector (FID) and a thermal conductivity detector (TCD). The Faradaic efficiency of CO product was calculated as:

$$FE(\%) = \frac{J_{co}}{J_{tot}} \times 100\% = \frac{n_{co} \times N \times F}{I \times t} \quad \text{(S1)}$$

where

J_{co}: partial current density toward CO production;

J_{tot}: total current density;

N: number of electrons transferred, which is 2 for CO;

n_{co}: the production rate of CO (measured by GC);

F: Faradaic constant, 96485 C·mol^{-1}

Turnover frequency (TOF) was estimated based on the following equation:

$$TOF\left(h^{-1}\right) = \frac{CO_{molecule/h}}{Ni_{atom}} = \frac{I \cdot t \cdot FE_{CO} \cdot M_{Ni}}{n \cdot m_{catalyst} \cdot w_{Ni} \cdot F} \quad \text{(S2)}$$

where

$CO_{molecule/h}$: the number of CO molecules produced in 1 h;

Ni_{atom}: the number of active Ni atoms in the catalyst;

J: the total current density of CO_2RR at a specific potential;

t: reaction time, 1 h (3600 s);

FE_{CO}: Faradaic efficiency of CO;

M_{Ni}: relative molecular mass of Ni;

n: the number of transferred electrons required to produce a CO molecule;

$m_{catalyst}$: the quality of the catalyst in the reaction;

w_{Ni}: the mass fraction of active Ni in the catalyst;

F: Faraday's constant (96485.33289 C·mol^{-1}).

The TOF calculated by Eq.(S2) reflects the conversion efficiency of the electrocatalytic reduction of CO_2 to CO on a single NiPc molecule per unit time. The TOF of the as-synthesized NiPc molecular catalysts is shown in Tab.S3. It is found that the TOF of Ni-G is the largest, which is consistent with the linear polarization curve after normalization.

1.7 CO_2RR Kinetics analysis

Assuming single Ni atom in NiPc is the active site in the CO_2-to-CO electro-reduction, the elementary reaction steps and enrolled reaction rate equations are listed in Table S1. The control equations are listed in Table S2. Here, r is the elementary reaction rate [$mol \cdot m^{-2} \cdot s^{-1}$], K is the reaction rate constant [$mol \cdot m^{-2} \cdot s^{-1}$], c is the concentration [$mol \cdot m^{-3}$], and θ is coverage, α is the symmetry coefficient, η is the overpotential [V], R is the gas constant [$J \cdot mol^{-1} \cdot K^{-1}$], T is the temperature [K]; θ subscripts CO_2 and COOH represent the intermediates $CO_{2,ads}$ and $COOH_{,ads}$, respectively; c subscripts CO_2 and HCO_3 represent the reactant CO_2 and electrolyte $KHCO_3$, respectively.

Table S1. Elementary reaction steps and reaction rate equations for the CO_2-to-CO electro-reduction on Ni atom.

$M_1 + CO_2 \underset{K_{102}}{\overset{K_{101}}{\rightleftharpoons}} M_1CO_{2,ads}$	(TS1.1)
$M_1CO_2 + CO_2 + H_2O + e^- \underset{K_{202}}{\overset{K_{201}}{\rightleftharpoons}} M_1COOH_{ads} + HCO_3^-$	(TS1.2)
$M_1COOH_{ads} + CO_2 + e^- \underset{K_{302}}{\overset{K_{301}}{\rightleftharpoons}} M_1 + CO + HCO_3^-$	(TS1.3)
$r_1 = K_{101} \cdot \left(1 - \theta_{CO_{2,ads}} - \theta_{COOH_{ads}}\right) \cdot \left(\frac{P_{CO_2}}{P^{\Theta}}\right)$	(TS1.4)
$r_{-1} = K_{102} \cdot \theta_{CO_{2,ads}}$	(TS1.5)
$r_2 = K_{201} \cdot \theta_{CO_{2,ads}} \cdot \left(\frac{c_{CO_2}}{c^{\Theta}}\right) \cdot \exp\left(\frac{\alpha F \eta}{RT}\right)$	(TS1.6)
$r_{-2} = K_{201} \cdot \theta_{COOH_{ads}} \cdot \left(\frac{c_{HCO_3^-}}{c^{\Theta}}\right) \cdot \exp\left(-\frac{(1-\alpha) F \eta}{RT}\right)$	(TS1.7)

$$r_3 = K_{301} \cdot \theta_{COOH_{ads}} \cdot \left(\frac{c_{CO_2}}{c^{\Theta}} \right) \cdot \exp\left(\frac{\alpha F \eta}{RT} \right) \quad \text{(TS1.8)}$$

$$r_{-3} = K_{301} \cdot \left(1 - \theta_{CO_{2,ads}} - \theta_{COOH_{ads}} \right) \cdot \left(\frac{P_{CO}}{P^{\Theta}} \right) \cdot \left(\frac{c_{HCO_3^-}}{c^{\Theta}} \right) \cdot \exp\left(-\frac{(1-\alpha) F \eta}{RT} \right) \quad \text{(TS1.9)}$$

Table S2. Control equations for CO_2-to-CO electro-reduction on Ni atom.

$$C_{CO_2} \frac{d\theta_{CO_2}}{dt} = r_1 - r_{-1} - r_2 + r_{-2} \quad \text{(TS2.1)}$$

$$C_{COOH} \frac{d\theta_{COOH}}{dt} = r_2 - r_{-2} - r_3 + r_{-3} \quad \text{(TS2.2)}$$

$$C_{dl} \frac{dE}{dt} = j(t) - \left[\left(r_2 - r_{-2} \right) + \left(r_3 - r_{-3} \right) \right] \cdot F / n \quad \text{(TS2.3)}$$

Fig. S16 shows the experimental polarization curve of the CO_2-to-CO electro-reduction on NiPc molecular catalyst and the simulated one, as well as the coverage of intermediate $CO_{2,ads}$ obtained in the simulation. By fitting the kinetic model with experimental data, the kinetics parameters are listed in Tab.S4.

It is well known that the rate constants of the electrochemical elementary steps of the CO_2-to-CO electro-reduction reaction are overpotential dependent that increase with increasing current density. At the overpotential of 0.53 V (i.e., cathode potential of -1.09 V vs. SHE), the term $K_{201} \cdot \exp\left(\frac{\alpha F \eta}{RT} \right)$ and $K_{301} \cdot \exp\left(\frac{\alpha F \eta}{RT} \right)$ for Ni-G are 8.40×10^2 and 1.82×10^9 $mol \cdot m^{-2} \cdot s^{-1}$, respectively, which are higher than that of the constant K_{101}. In combined with the magnitude of the coverage of $CO_{2,ads}$, it can be therefore concluded that the elementary chemical step TS1.1 is the rate determining step.

1.8 Density functional theory calculation methods

All spin-polarized density functional theory calculations were implemented in the Vienna Ab initio Simulation Package (VASP).[4] The Projector augmented wave (PAW) pseudopotential and Perdew-Burke-Ernzerhof functional (PBE) of the generalized gradient approximation (GGA) were applied to describe the interactions between valence electrons and ionic cores, and the exchange-correlation effects.[5, 6] The wave function calculations were based on the kinetic energy cutoff of 500 eV with the

smearing width of 0.1 eV. The supercell of 9 × 9 and the vacuum gap of about 15 Å were used for negligible interactions between the system and its mirror images. The van der Waals interaction was described through zero damping DFT-D3 method of Grimme.[7] Moreover, the solvent model was also considered for the binding energy of NiPc, where H_2O was used as the solvent with the dielectric constant of 78.4. The geometry relaxation was stopped if the total energy change and forces between two steps were smaller than 1×10^{-5} eV and 0.05 eV/Å, respectively. Concerning the properties of charge transfer, atom charges were considered via the Bader charge analysis.[8]

According to the report of Gao et al.,[9] to simulate the experimental synthesis of carbon nanotubes (CNTs) with diameters of 20 nm and 40 nm, the bending graphenes, with two kinds of curvatures, corresponding to the CNTs with the diameters of 20 Å and 40 Å, were applied, as shown in Fig. S13. For the adsorption of NiPc on different carbon supports, three traditional adsorption sites and two adsorption configurations were considered, as shown in Fig. S14. The optimal adsorption site and configuration were chosen for further study and the binding energy of NiPc (E_b) on different CNTs and graphene was determined by:

$$E_b = E_{catalysts} - (E_{sub} + E_{NiPc}) \quad \text{(S3)}$$

where $E_{catalysts}$, E_{sub}, E_{NiPc} are total energies of NiPc adsorbed on substrate, substrate (different CNTs and graphene), and NiPc molecule, respectively. The adsorption energy of CO_2 (E_{ad}) on different catalysts was defined as:

$$E_b = E_{CO_2}{}^{*} - (E_{catalysts} + E_{CO_2}) \quad \text{(S4)}$$

where $E_{CO_2}{}^{*}$ and E_{CO_2} are the total energies of CO_2 adsorbed on catalyst and CO_2 molecule, respectively.

2. Supplementary Figures and Tables

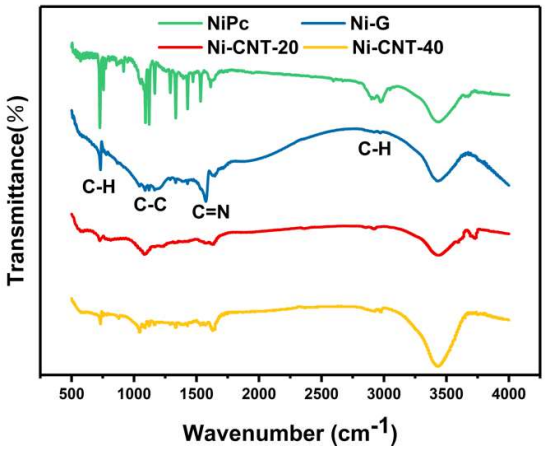

Figure S1. FTIR spectra of NiPc, Ni-G, Ni-CNT-20 and Ni-CNT-40.

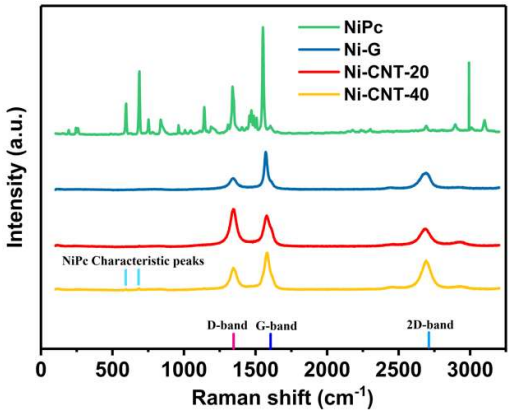

Figure S2. Raman spectra of NiPc, Ni-G, Ni-CNT-20 and Ni-CNT-40.

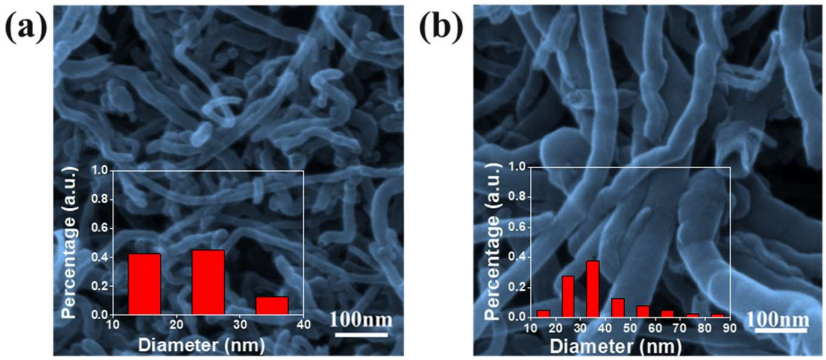

Figure S3. SEM images of (a) Ni-CNT-20 and (b) Ni-CNT-40. The measured average diameter statistics is shown in the inset figure.

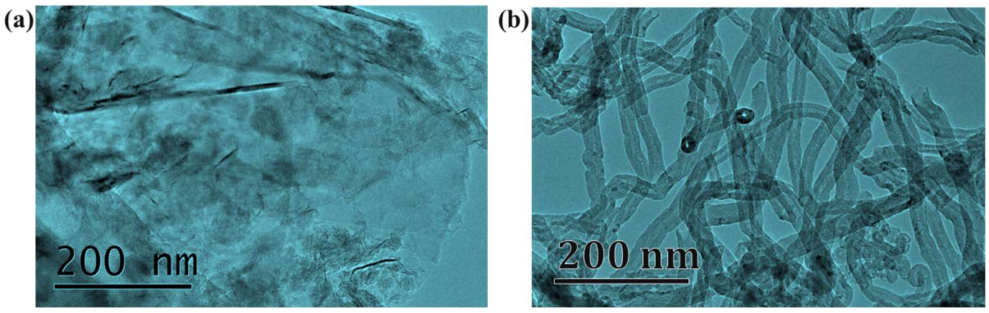

Figure S4. TEM images of (a) Ni-G and (b) Ni-CNT-20, scale bar 200nm.

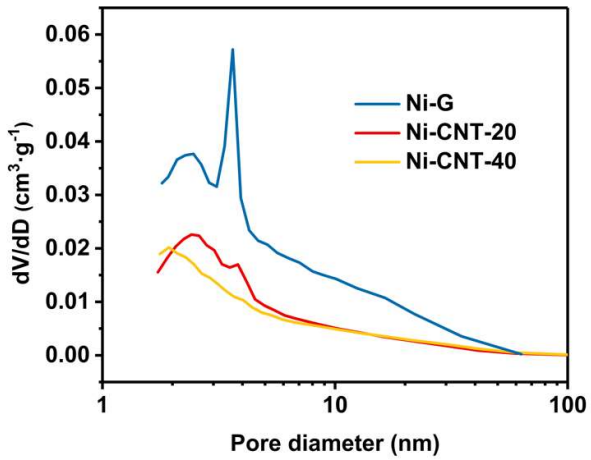

Figure S5. Pore size distribution. The micropore volume is 0.096 cc·g^{-1}, 0.054 cc·g^{-1} and 0.041 cc·g^{-1} for Ni-G, Ni-CNT-20 and Ni-CNT-40, respectively.

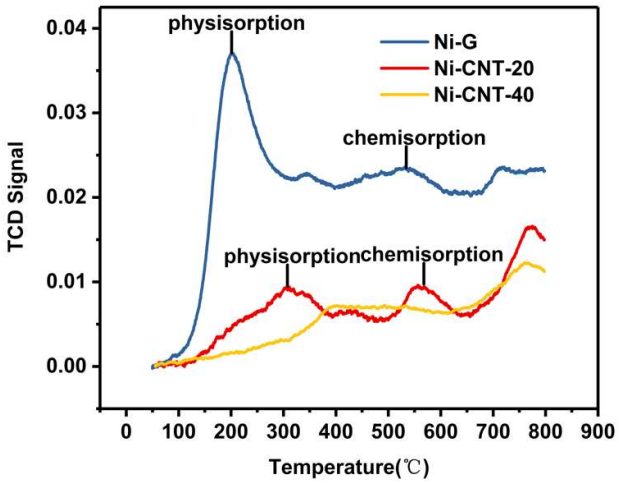

Figure S6. Temperature programmed desorption (CO_2-TPD) curve for Ni-G, Ni-CNT-20 and Ni-CNT-40.

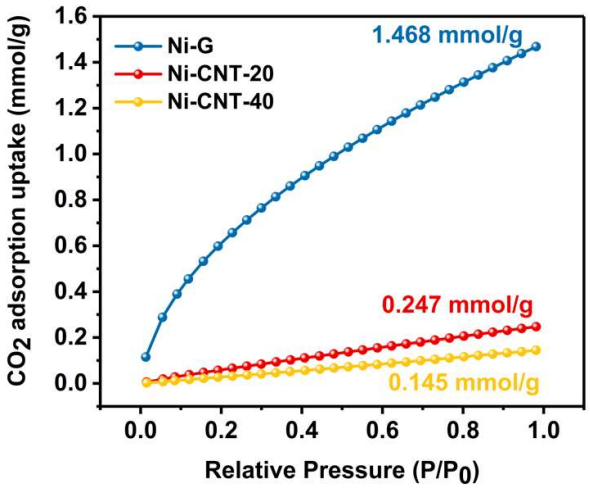

Figure S7. CO_2 physical adsorption curves for carbon supports

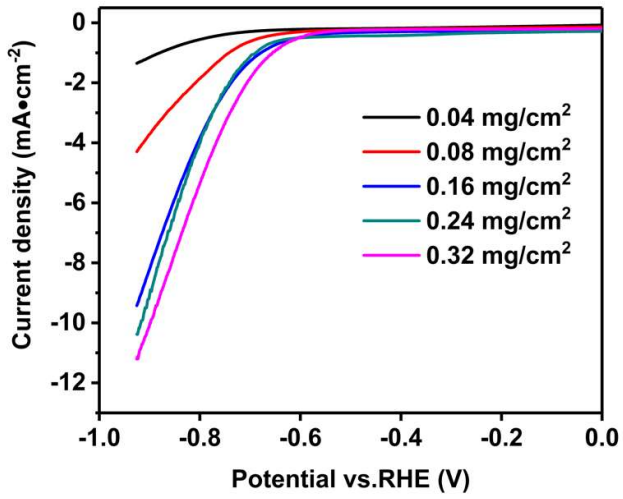

Figure S8. Study of catalyst loading on the performance of CO_2RR in CO_2-saturated 0.5 M $KHCO_3$ solution.

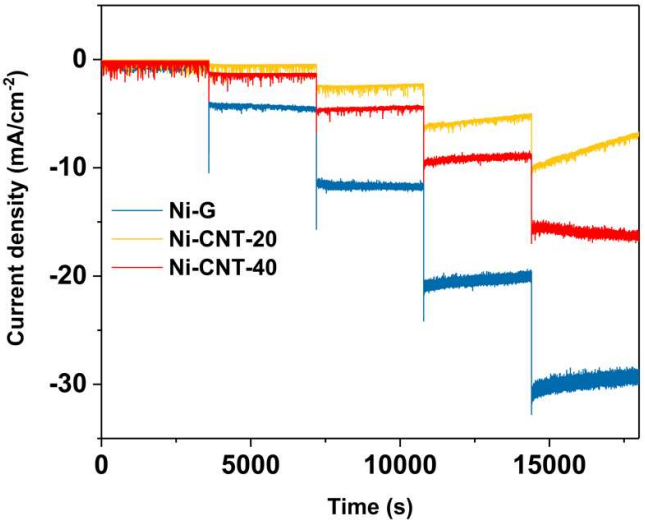

Figure S9. Controlled potential electrolysis at different applied potentials.

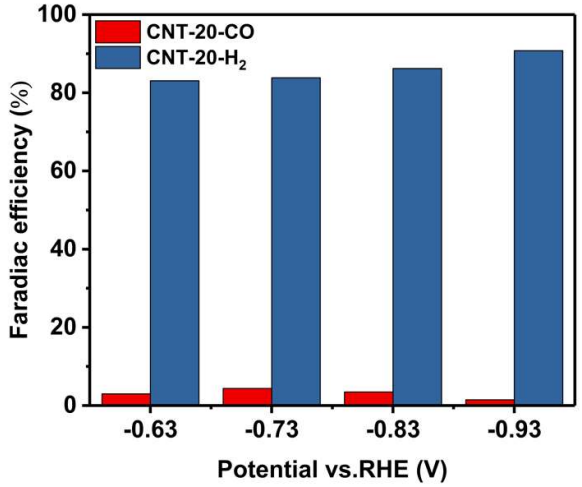

Figure S10. Faradaic efficiency of CNT-20 at -0.53 to -0.93V vs. RHE.

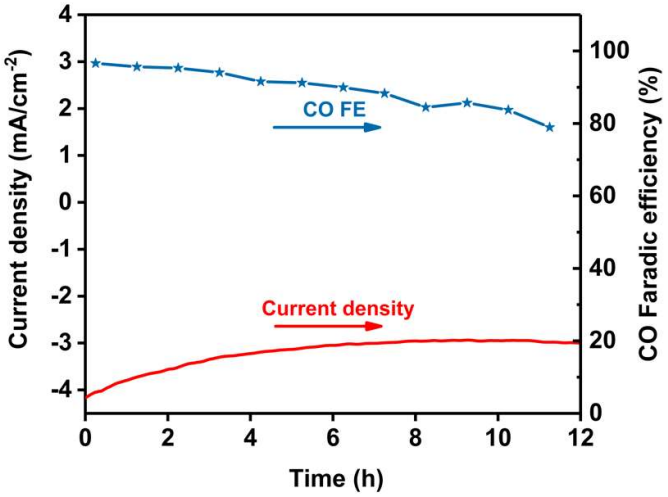

Figure S11. Stability test of Ni-G at -0.63 V vs. RHE in 12 hours.

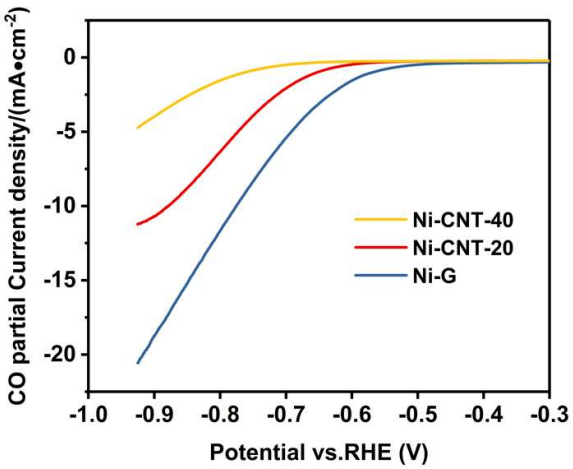

Figure S12. Potential dependent CO partial current density curve for Ni-G, Ni-CNT-20 and Ni-CNT-40.

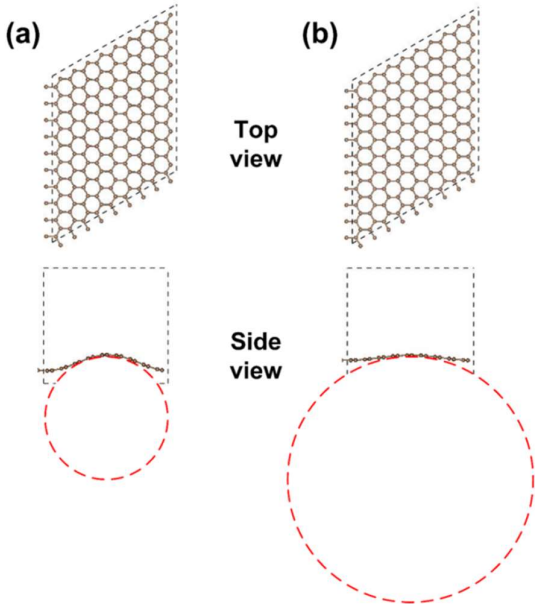

Figure S13. Top and side view geometric optimization structure of (a) CNT-20 and (b) CNT-40.

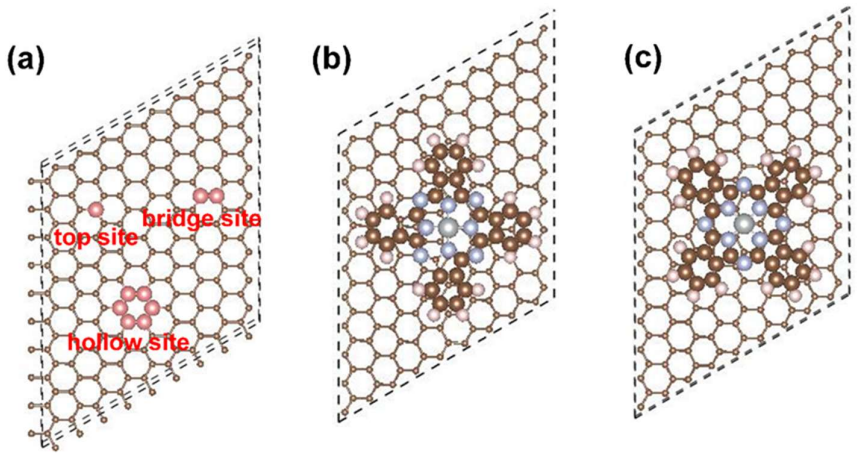

Figure S14. (a) Three adsorption sites (top, bridge, and hollow sites). (b-c) two adsorption configurations of NiPc on carbon nanotubes and graphene.

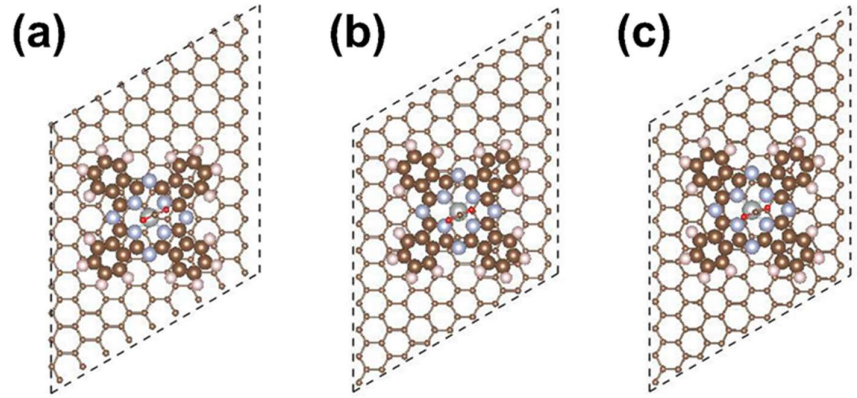

Figure S15. Top view geometric optimization structure of CO_2 adsorbed on (a) Ni-G, (b) Ni-CNT-40, and (c) Ni-CNT-20.

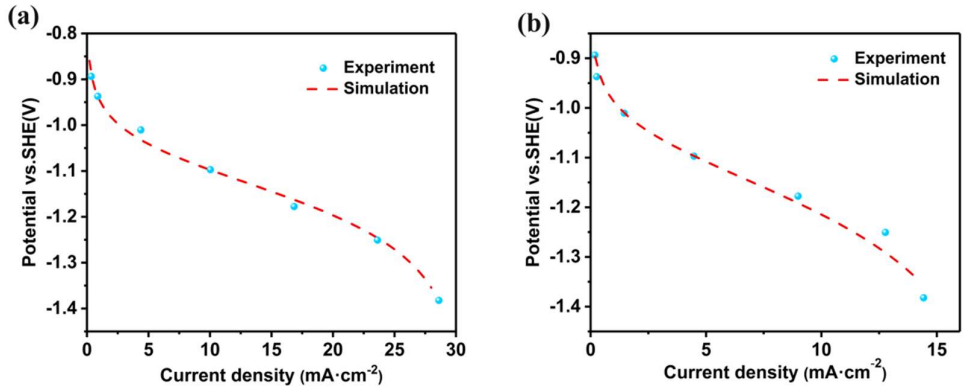

Figure S16. The CO-partial J-V curve of (a) Ni-G and (b) Ni-CNT-20. (these data were obtained from kinetics simulation).

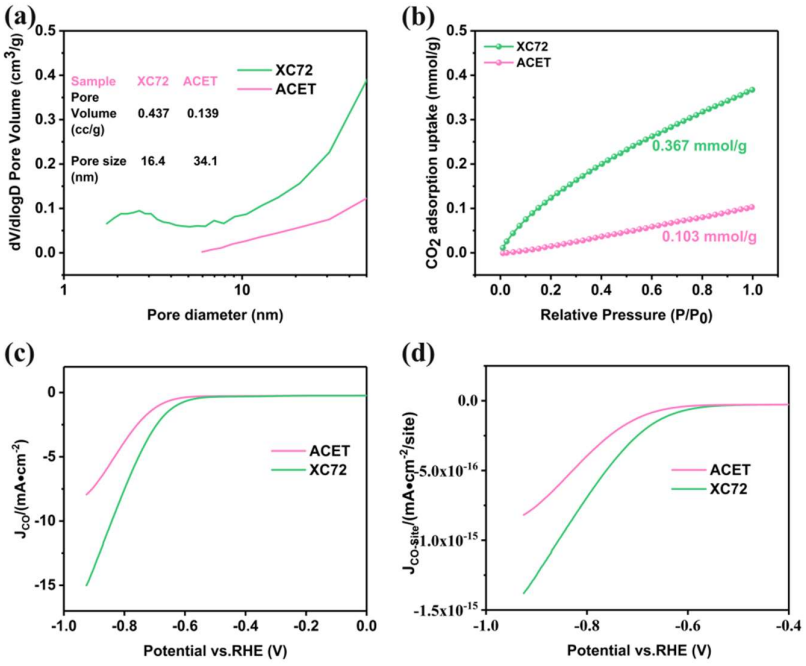

Figure S17. (a) Pore size distribution. (b) CO_2 adsorption isotherm. (c) Potential dependent CO partial current density. (d) Potential dependent CO partial current density normalized to number of active sites.

Note: To further support our conclusion, we immobilized NiPc onto two different types of three-dimensional (3-D) carbon spheres. It is found that with increase of the microporous structure in the carbon spheres, the CO_2 physical adsorption capacity enhances, which thereby increases the surface concentration of CO_2 and boosts the CO_2RR activity

Table S3. Turnover frequency (TOF) calculation for catalysts.

Catalyst	Potential (V vs. RHE)	Current density (mA • cm^{-2})	Faradaic efficiency (%)	TOF (h^{-1})
Ni-G	-0.83	20.46	82.55	6089.53
Ni-CNT-20	-0.83	9.17	98.815	2110.63
Ni-CNT-40	-0.83	5.66	100	582.19

Note: TOF calculation formula was shown in equation S2.

Table S4. Kinetic constant fitting.

Kinetic constant step	Cathode kinetic constant for Ni-G	Cathode kinetic constant for Ni-CNT-20
K_{101}	1.95e+02	9.95e+01
K_{102}	4.38e-01	4.13e+01
K_{201}	1.75e-06	1.06e-05
K_{202}	3.13e-02	8.15e-01
K_{301}	3.79e+00	2.29e+00
K_{302}	8.76e-03	5.43e-02

Note: The reaction mechanism equation and the conversion formula of cathode kinetic constant and kinetic constant were shown in Tab. S1.

Notes and references

1. Q. Mao and U. Krewer, Electrochim. Acta, 2013, 103, 188-198.
2. Q. Mao, U. Krewer and R. Hanke-Rauschenbach, Electrochem. Commun., 2010, 12, 1517-1519.
3. Q. Mao and U. Krewer, Electrochim. Acta, 2012, 68, 60-68.
4. G. Kresse and J. Furthmuller, Phys. Rev. B: Condens. Matter Mater. Phys., 1996, 54, 11169-11186.
5. P. E. Blochl, Phys. Rev. B: Condens. Matter Mater. Phys., 1994, 50, 17953-17979.
6. J. P. Perdew, K. Burke and M. Ernzerhof, Phys. Rev. Lett., 1996, 77, 3865.
7. S. Grimme, J. Antony, S. Ehrlich and H. Krieg, J. Chem. Phys., 2010, 132, 154104.
8. W. Tang, E. Sanville and G. Henkelman, Phys. Rev. B: Condens. Matter Mater. Phys., 2009, 21, 084204.
9. W. Gao, T. Ting Cui, Y. Fu Zhu, Z. Wen, M. Zhao, J. Chen Li and Q. Jiang, Sci. Rep., 2015, 5, 15095.